Received: 7 September 2023 | Revised: 24 November 2023 | Accepted: 8 January 2024 | Published online: 15 January 2024

RESEARCH ARTICLE

Archives of Advanced Engineering Science

yyyy, Vol. XX(XX) 1–9

DOI: 10.47852/bonviewAAES42021702

# Real Time Route Adjustment of a UAV Based on Dust Measurement with an Onboard Sensor

**Roberto Diego Martinez**[1,*], **Alejandro Morales**[2]

*1 AP Division, The Institute for Energy and the Environment, Brazil.*

*2 Institue of Advanced Studies, University of São Paulo, Brazil.*

***Corresponding author:** Roberto D. Martinez, AP Division, The Institute for Energy and the Environment, Brazil. Email: rdmartinez@usp.edu.br

**Abstract:** This research is driven by a pressing requirement to improve the effectiveness and safety of unmanned aerial vehicle (UAV) operations, specifically in atmospheric particle sensing. Airborne particulates present a substantial health hazard, leading to an increasing demand for inventive solutions capable of autonomously guiding UAVs along optimal routes, steering clear of regions with heightened dust concentrations. This research aims to address this challenge by developing a sophisticated approach that integrates atmospheric particle sensors with UAV flight control systems. The approach outlined in this study relies on atmospheric sensors mounted on a UAV to measure dust levels in a specified region. The UAV, following a predetermined route over the area, detects dust pollution. It dynamically adjusts its route based on the observed dust levels, avoiding areas with high concentrations of dust. This adaptive route determination aims to identify safe paths, avoiding regions with elevated dust levels that may pose risks to human health. The flight strategy and area-scanning methodology tailored for this objective are established, enabling the UAV to execute the assigned task. The ultimate goal is to create a system that not only minimizes energy consumption but also prioritizes human health by autonomously redirecting the UAV away from potentially harmful dust levels. The real-time monitoring and telemetry data feedback mechanisms further contribute to the advancement of UAV technology for environmental sensing and risk mitigation. Additionally, the integration of the laser-based dust sensor, i.e., Gp2y10, with the ArduPilot autopilot flight computer ensures seamless coordination, with the UAV adjusting its flight path based on the sensor's output.

**Keywords:** unmanned aerial vehicle, route planning, atmospheric measurement, aerial monitoring

## 1. Introduction

With the increasing prevalence of Unmanned Aerial Vehicles (UAVs), diverse application areas are emerging. UAVs are now effectively employed for purposes such as reconnaissance (Wang et al., 2022; Bakirci & Ozer, 2023a; Loli et al, 2022), traffic management (Aissaoui et al., 2023; Masuduzzaman et al., 2022), surveillance (Ramachandran & Sangaiah, 2021; Bakirci & Ozer, 2023b), target tracking (Li et al., 2021; Wang et al., 2022), logistics (Song et al., 2018; Hossain et al., 2022), disaster and accident response (Yu & Xing, 2021), and more (Xin et al., 2022; Malamiri et al., 2021). The proliferation of sensors on these vehicles is reshaping and expanding their capabilities. Ongoing studies aim to enable UAVs to autonomously execute their designated missions. One crucial area of research in this context is route planning (Puente-Castro et al., 2022), which remains an active and multifaceted field, utilizing various methods to address the challenges posed by this intricate task.

Furthermore, the utilization of UAV technology for air quality monitoring and measurement is gaining widespread recognition. A comprehensive analysis is presented in Lambey and Prasad (2021), emphasizing that UAVs, equipped with atmospheric sensors and sampling devices, enable more precise and comprehensive air quality measurements. Traditional air quality measurement methods often rely on stationary and limited monitoring stations, which have limitations in capturing the spatial and temporal variability of pollution and require skilled personnel. To overcome these challenges, the study underscores the importance of real-time systems with higher spatial and temporal resolutions. It highlights the emergence of UAVs equipped with various sensors as a promising solution for on-site air quality surveillance, offering new possibilities for studying air pollution, emissions, and environmental changes.

Villa et al. (2016) explores current applications and future perspectives of UAVs in air quality monitoring. The paper discusses the use of small UAVs equipped with various sensors for in-situ air quality monitoring and its potential benefits. Traditional air quality assessments relying on ground-based monitoring, manned aircraft, and satellites may not always be suitable for collecting data near pollution sources due to site complexity, moving sources, or physical

barriers. The review's objectives were twofold: to gather information on the application of UAVs in air quality studies and to evaluate their advantages and range of applications. The paper concludes that UAVs hold significant potential for air quality research, but several challenges must be addressed, including enhancing flight endurance, payload capacity, sensor accuracy and dimensions, and sensitivity. Importantly, the authors note that challenges extend beyond technology and encompass policy and regulations, which vary between countries and present the primary hurdle to the broader use of UAVs in atmospheric research.

In Jońca et al. (2022), it is demonstrated that UAVs can quickly and effectively measure air quality over a wide geographical area through their sensors. The study addresses current challenges and limitations in the atmospheric pollution monitoring processes of UAVs, emphasizing factors such as energy consumption, the effect of weather conditions, sensor accuracy, and data analysis.

In Lambey and Prasat (2021), the effective utilization of UAVs for atmospheric measurements in expansive regions is demonstrated through numerical analysis. The author outlines a strategy for creating a comprehensive map of an entire region by subdividing areas, too extensive for a single UAV to cover, into smaller, manageable sub-areas. Each of these smaller sections is then independently scanned by the UAV. Furthermore, the study delves into determining the optimal speed for UAVs, highlighting that more consistent results were attained by extending the flight time of the UAVs.

Sziroczak et al. (2022) discusses how small UAVs contribute to road weather management processes and their advantages over existing measurement methods. The study evaluates the current state of road weather management using small UAVs and highlights the potential of this technology. Li et al. (2022) provides insights into effective coverage of flight mission zones through a different strategy for flight plan creation. Additionally, there are studies in the literature where route planning and task distribution for UAVs are carried out using different algorithms (Cui & Wang, 2021).

This research aims to address the aforementioned challenge by developing a sophisticated approach that integrates atmospheric particle sensors with UAV flight control systems. The principal goal is to establish a system that not only minimizes energy consumption but also prioritizes human health by autonomously steering the UAV away from regions exhibiting potentially harmful levels of dust. The inclusion of real-time monitoring and telemetry data feedback mechanisms enhances the progress of UAV technology in environmental sensing and risk mitigation. Moreover, the seamless coordination is ensured by integrating the laser-based dust sensor with the ArduPilot autopilot flight computer, allowing the UAV to adapt its flight path based on the sensor's output.

The significance of this research resides in the development and experimentation of diverse missions aimed at refining the UAV's path using dust sensor measurements. The autopilot system intelligently directs the UAV away from locations with heightened dust levels, thereby reducing potential risks to human health. Throughout this process, the UAV's flight speed, altitude, and sensitivity to wind conditions are meticulously considered, ensuring adherence to the assigned mission area and initial position. The utilization of a UAV for measurements using an atmospheric dust sensor in precise route applications yields significant benefits, particularly in air quality measurement and route planning. This technology enables UAVs to navigate with heightened accuracy and provides more precise measurements of air pollution. Notably, the system's cost-effectiveness and simple hardware structure enhance accessibility and utility, making it an invaluable tool for a wide range of applications.

## 2. Research Methodology

### 2.1. Flight planning and execution

The flight planning for the UAV is facilitated by Mission Planner, a widely utilized open-source software tool. Functioning as ground control station software, Mission Planner serves purposes such as mission planning, UAV configuration, and real-time telemetry monitoring. It is compatible with diverse UAV types, encompassing fixed-wing, multi-rotor, and VTOL aircraft. Within Mission Planner, users have the capability to chart out missions by specifying waypoints, configuring altitudes, and adjusting various mission parameters. Additionally, the software offers real-time monitoring features, displaying the UAV's current location, battery level, and other essential data.

Since Mission Planner is a powerful software tool that allows planning and execute autonomous flights with various types of UAVs, it is necessary to detail the steps it follows. In this context, the process is started by connecting the UAV to the computer and activating the Mission Planner. After connecting to the UAV with the Mission Planner interface, the map view is used to plan the flight path with “Flight Planning”. After the boundaries of the area to be examined are determined with the area creator function, the mesh option from the flight plan menu allows a grid of waypoints to be followed by the UAV to capture the images of this area. Here, “sld” and “iptf” are used to set the altitude, speed and other parameters of the flight plan. After the flight plan is created, it is activated to save the plan to the flight controller of the UAV. It is now possible to switch to the “Flight Data” tab to monitor the progress of the UAV during the flight. After completing its mission, the UAV returns to the launch point and can land automatically.

However, using the ArduPilot flight controller to plan a mission with the dust sensor (GP2Y10) connected to the computer during the mission creates a specific situation. For this, all systems are connected and a new mission is created with the “New Plan” option in the “Flight Plan” tab on Mission Planner. From there, waypoints can be added to the mission by clicking on the map or entering specific coordinates. To include the GP2Y10 sensor in the task, a command item is added to the task by selecting the “Command” item from the drop-down menu with the “Add Item” command. From there, “Sensor” is selected as the command type and GP2Y10 sensor is selected from the list of available sensors. After adding the GP2Y10 sensor to the mission, the desired dust level threshold can be set and

actions to be taken such as changing the flight path or triggering a warning can be determined when the threshold is exceeded.

## 2.2. Area coverage

The challenge lies in the drone's inability to cover the entire target area in a single flight due to limited power capacity. Typically, drones have an average flight time of around 30 minutes. When dealing with expansive target areas that exceed the drone's current battery capacity, we adopt a strategy of dividing the target region into smaller sections to ensure comprehensive coverage. In such instances, we propose employing the polygonal decomposition method, outlined below, to effectively partition the entire area.

The area decomposition problem, where UAVs have to divide a given area into $i$ parts to completely cover an area, is important for the UAV workspace division. In our presented scenario, $i$ UAV scan areas placed at different $P_n$ origins are divided into segments with $P_i$, containing a specific area and a specific point within the $A_P$ area. In order to completely cover the UAV given area, the $A_P$ must be divided according to the scanning capacity and relative capabilities of the UAV. In the assigned area, each UAV scans its area using the segment coverage algorithm. This section examines the algorithm used in a scenario with a convex area $A_P$ and no obstacles. A generalized version can handle non-convex and simply unconnected areas, but adds computational complexity. In addition, the fact that the lands where atmospheric measurements are performed generally have a concentric elevation and do not contain obstacles are effective in the implementation of this scenario. However, using the maximum range of UAVs only as a criterion may not ensure the efficient fulfillment of the mission. Because the range of UAVs is also related to flight time, energy consumption and other factors. Therefore, a more sophisticated approach is required to consider the full capabilities of UAVs and to allocate the area to cover it in the most efficient way. This approach can be achieved using an optimization algorithm or artificial intelligence methods that take into account the characteristics of UAVs, mission requirements and other factors in the field.

In this context, depending on the system capacity of the UAV, it is defined which part of the $P$ region will be allocated for a mission flight. These ratios are expressed by the set of $k_n$, $n = 1,\dots,i$ values $0 < k_n < 1$ and $\sum_{n=1}^{i} k_n = 1$. Thus, the problem addressed is as follows. Given an area $A_P$ and $i$ sites, sub-areas $P_1 \dots, P_i$ divide $A_P$ into $i$ non-overlapping areas. Such that the area of $A_{P,n}$ is expressed as the ratio multiplied by the area of the relevant area $k_n \times S(A_P)$, and $P_n$ is on $A_{P,n}$. Let each region of the $A_P$ area is scanned by the UAV and the UAV is assigned to one of $P_1 \dots, P_i$. In this case, $P_1 \dots, P_i$ is a set of sites, for each of which the required field is specified a field requirement called $S_R(P_n)$.

$A_P$, an r-point area, is defined as an area $A_P$ containing $r$ points, and the required area $S_R(P(A_P))$, where $S_R(P(A_P)) = S_R(P_n)$, expresses the sum of the areas claimed by $A_P$ is called a completed field. As mentioned earlier, $A_P$ is considered a convex and solid area. In this case, the desired area segment is divided into two as r-point ($r > 0$) full area domain and $r_1$ and $r_2$-point full area domains, $r_1 + r_2 = r$ and $r_1, r_2 > 0$, which can be obtained using line segment $i - 1$. The calculation of each piece is based on the zigzag pattern approach. This procedure is called exactly $i - 1$ times to divide by $i$ convex, 1-full area.

For a scanning mission, a UAV scans the designated area to capture measurements. This area is defined by a fixed Earth Coordinate System (ECS). The sensors enable UAVs to determine their local coordinates and those of objects. Each UAV is associated with a Vehicle Coordinate System (VCS) that adjusts the starting point and direction based on its motion (x-axis forward, y-axis left, z-axis up). The VCS is oriented in the vertical plane and specified by -α relative to the horizontal axis. Assuming a flat terrain, when the UAV moves along a horizontal plane and measures between waypoints, the scanned area forms a pyramid on the land, as depicted in Figure 1. Here, U and V represent the x and y velocity components of the drone, respectively. In this scenario, the detection width of a UAV flying in the vertical plane of the VCS is illustrated in (1).

$$\mathrm{f} = 2\mathrm{W}_{\mathrm{VCS}} \tan\gamma \left[\sin\alpha + \cos\alpha \times \tan\left(\frac{\pi}{2} - \alpha - \beta\right)\right] \quad (1)$$

$W_{VCS}$ denotes the UAV's height, while the β and γ angles define its scanning area. The planar algorithm relies on a zigzag pattern to cover a given area, calculating the distance between parallel line segments using (1) as the initial approximation. To generalize this planar algorithm to the considered 3D medium, the non-planar area must be an x-z projected planar surface. When deploying the UAV to a defined area (a convex polygon corresponding to $A_P$), a procedure is needed to include that specific area in target identification. Our curved areas are effectively covered with the zigzag pattern, a faster method than the spiral pattern, in rows perpendicular to the scanning direction. The time to cover the field is calculated based on the time to move through these rows, yielding lines of approximately equal distance in any alternative scanning direction. However, as depicted in Figure 2, a significant variation may be required for the total number of turns. Therefore, when measuring the height of the area along the UAV's scanning direction, the rotation amount around an area with a similar ratio to this measurement should be minimized. It's important to note that the term "height of the area" simply refers to the altitude, and the flight altitude can also be indicated by it. The diameter function, *d(ϕ)*, can be used to calculate the height of the area (i.e., the UAV's altitude) along the scanning direction. If the diameter of an area is to be calculated for a defined value of $\phi$, that area is rotated by a certain amount, in this case, -$\phi$. Then, the diameter value is determined by measuring the distance between the extreme points. For a hatching direction in the α orientation, the height $dA_P(\alpha - \pi/2)$ of an area $A_P$ is in the α orientation.

**Figure 1**
**Determination of the measurement area with a scanning pyramid that intersects the terrain**

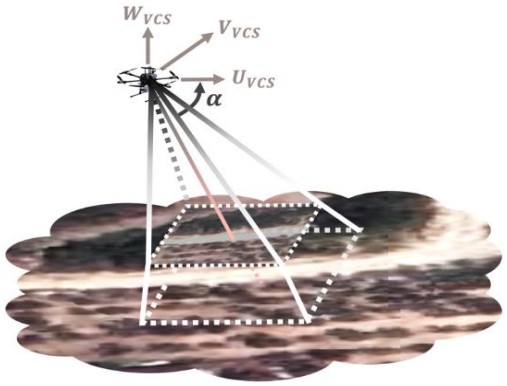


**Figure 2**
**Illustration of the number of turns required to cover an area in different scanning directions**

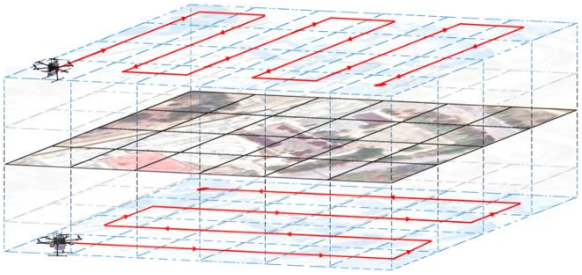

The cumulative height of the sub-regions is determined by multiplying the height of the area at that angle by ϕ for each *d(ϕ)* and adding the value of *d(ϕ)* for the hole to (2).

$$P(\phi) = dA_P(\phi) + \sum_n dh_n(\phi) \qquad (2)$$

where $dA_P(\phi)$ represents the diameter function of the perimeter and each hole $dh_n(\phi)$. The optimal partitioning is identified by the scanning direction $\alpha = \phi + \frac{\pi}{2}$, which minimizes P. Referring to Figure 3, the form of the d(ϕ) for an area can be derived by computing the average height of that area moved randomly between two parallel plates. Specifically, the closest points of the area to these plates are determined for all random configurations, and the distances between these determined points are measured and averaged. Increasing the number of measurements provides more accurate results. Therefore, *d(ϕ)* for a convex area with i sides is expressed in (3).

$$d(\phi) = \begin{cases} c_1 \sin(\phi + \theta_1) & \phi \in [\phi_0, \phi_1) \\ c_2 \sin(\phi + \theta_2) & \phi \in [\phi_1, \phi_2) \\ \vdots & \\ c_{2i} \sin(\phi + \theta_{2n}) & \phi \in [\phi_{(2i-1)}, \phi_{2n}) \end{cases} \qquad (3)$$

where, $d(\phi)$ of a rotated area is piecewise sinusoidal and is controlled by the constants $c_1$ and $\theta$. This creates reset points $\phi_0 = 0$ and $\phi_{2n} = 2\pi$.

The minimum value of *d(ϕ)* is identified when one edge of the circumference is horizontal ($dA_P{}' < 0$) or at the zero points. In contrast, for a random point between the plates, $dA_P{}'' < 0$ there may be a maximum value, as indicated in (4). Therefore, the minimum occurs at points where the scanning direction is parallel to one side of the circumference, and these directions can be determined through testing.

$$P''(\phi) = dA_P''(\phi) + \sum_n dh_n''(\phi) < 0 \qquad (4)$$

The diameter function assesses the height of individual points on an object's surface. In computing *d(ϕ)* for an area, the outlined method gauges the maximum distance between the area's extreme points. This approach is applicable to more intricate shapes, allowing for the calculation of *d(ϕ)* values by measuring the height along each side of an area.

**Figure 3**
**Formation of the diameter function by rounding the area**

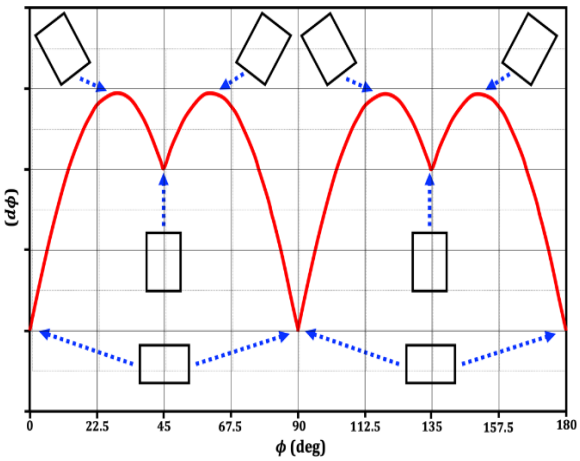


The same methodology is also applicable to more complicated areas with obstacles such as trees, tall buildings, communication towers, and lattice-structured electrical distribution towers. In such scenarios, the total *d(ϕ)* of the objects' circumferences is employed to minimize altitude of the unmanned aerial vehicle. The computation of the complete partitioning of a convex i-area $A_P$, with m representing the number of vertices, demands time $T(i-1)(i+m)$. Subsequently, the unmanned aerial vehicle is allocated to the derived areas in a specific sequence. To align with the zigzag pattern of each scanning flight of the aerial vehicle, the scanning direction should be optimized to minimize the overall number of turns around the entire area. This entails determining various directions based on the number of sides of the acquired area, $A_{P,n}$, and sequentially testing each direction. Consequently, three distinct areas are designated to scan an area, and the unmanned aerial vehicle survey the region defined by a seven-sided polygon illustrated in Figure 4.

**Figure 4**
**Area division results**

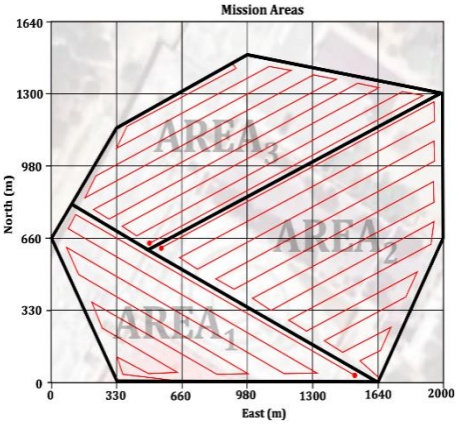


## 3. System Verification

During the evaluation process, test measurements were carried out in the standard ambient room (temperature 24°C-26°C, 60%-61% relative humidity) for ten minutes. Data were recorded at regular intervals using the 3443 Kanomax powder monitor for the designed caliber. System performance, $P_s$, is calculated by (5) as follows.

$$P_s = \frac{C_m - C_s}{C_m} \times 100\% \quad (5)$$

where $C_m$ represents the PM2.5 concentration measured by the dust monitor, while $C_s$ represents that of the designed system. Before filtration, the average PM2.5 concentration measured by the dust monitor was 19.4 μg/m$^3$, while the measurement of the GP2Y10 sensor was 10.5 μg/m$^3$. The measured difference between the two equipment was 7.6 μg/m$^3$. After system filtration, the dust monitor measured the PM2.5 concentration at an average of 22.1 μg/m$^3$, while the average concentration measured by the GP2Y10 was 15.8 μg/m$^3$. The measured concentration difference between the devices was recorded as 6.3 μg/m$^3$. In Figure 5, the status shown in red represents the pre-filtering status, while the green color represents the post-filtering values.

**Figure 5**
**Measured PM2.5 concentrations for filtration**

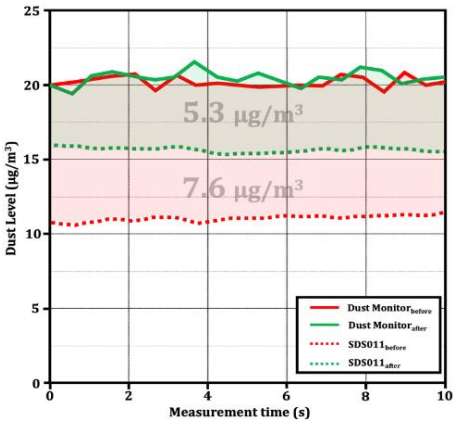


Figure 6 shows the measured PM2.5 concentration relationship between the dust monitor and the designed system. The measured PM2.5 concentrations show a linear relationship with the values measured by the dust monitor with the correlation equation $y = -0.19x + 17.4$ for the standard system, while $y = 1.07x + 4.18$ for the system after optimizations. The designed systems have a linear correlation with the verification equipment.

### 3.1. Field scanning

For the field survey application, atmospheric measurement in a $10^2$m field is considered. Then, the area of $10^2$m is divided into areas of $2^2$m, and it is first requested to scan an area of 10 meters in the vertical plane. Next, it slides on the block next to it 2 meters and performs the scanning process. After scanning in the opposite direction on this vertical plane, this area scanning process is completed so that the entire area is scanned. In other words, the hatch pattern starts at a corner and moves up and down in a vertical line, while moving 2 meters horizontally between each vertical line. When the final field is reached, scanning mode is completed. After going up to the first altitude of 50 meters and scanning the area in a zigzag pattern, the drone ascends to the next altitude level until it reaches 200 meters.

In Figure 7a and 7b, each square represents a 2m x 2m sub-square, and the entire scanning area is divided into 25 sub-squares arranged in a 5x5 grid. The zigzag pattern of the flight path is shown with diagonal lines. Figure 7a starts in the lower left corner of the UAV scanning area and moves diagonally upwards to the upper right corner. Then it moves diagonally down to the lower left corner of the next column until it reaches the upper right corner of the scanning area. As shown in Figure 7b, the UAV rises 50 meters after completing a tour and repeats the same pattern until it reaches an altitude of 200 meters.

**Figure 6**
**Linearity of performance for a calibrated dust sensor**

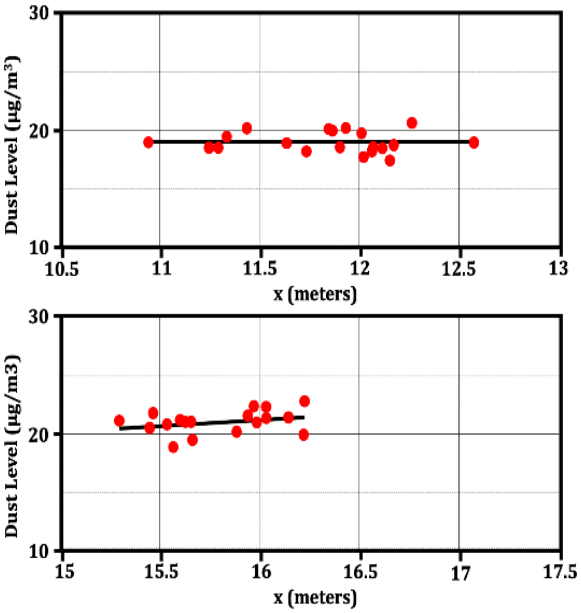


## 3.2. Real time routing

The GP2Y10 sensor, shown in Figure 8, used in this study, is an air quality sensor that measures the concentration of fine particulate matter in the air. Therefore, although it cannot provide direct information about a precise flight path, it can be used to measure the dust level at different points in the air during the flight. However, in order to use the GP2Y10 sensor to perform a precise flight path for a specific mission, a number of system improvements have been made by following the steps below.

**Figure 7**
**(a)Flight path planning (xy plane)**

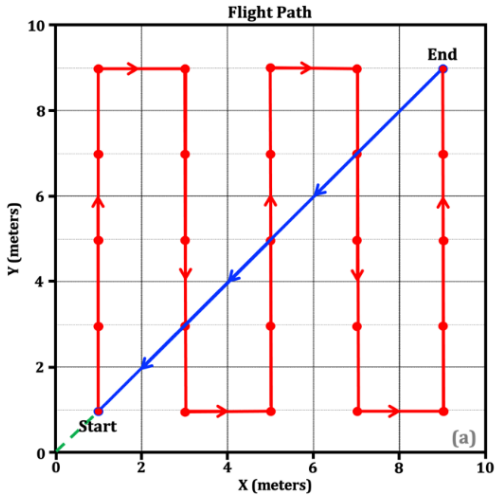


**(b)Flight path planning (xz plane)**

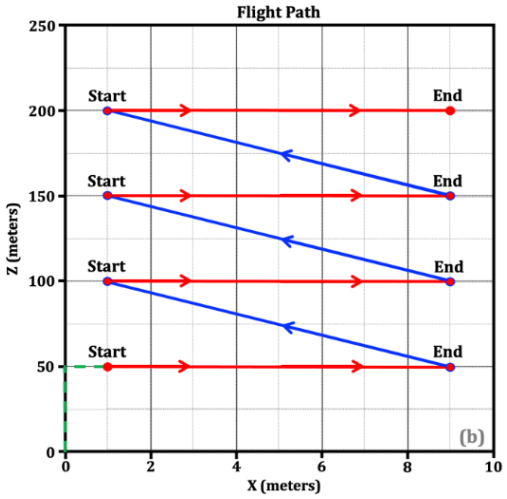


For example, if the sensor detects a high level of dust in a certain area, it can adjust the flight path through software to avoid that area. In doing so, the GP2Y10 dust sensor and autopilot system are first initialized. The dust concentration threshold in µg/m³ and the first flight mode are automatically set, and the original flight path for the drone is also determined. Then the algorithm enters a loop that will run forever. At each iteration, the dust concentration is read from the sensor and compared to this threshold. If the dust concentration exceeds the threshold, it switches to manual flight mode, calculates a new flight path to avoid high dust area, and determines the new flight path. If the dust concentration falls below the threshold, the original flight path is adjusted by reverting to automatic flight mode. A waiting period is also added before rechecking the dust concentration to prevent excessive readings from the sensor.

**Figure 8**
**The dust sensor (GP2Y10) module**

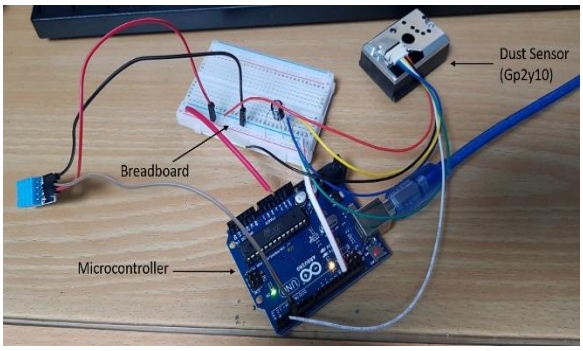


The threshold considered "pollution" for PM levels may vary depending on certain regulations or standards in a particular region or country. In general, the World Health Organization (WHO) defines PM2.5 levels above 25 µg/m$^3$ as unsafe for human health, while levels above 50 µg/m$^3$ are considered very high and pose a significant health risk. The flight path is planned by determining this limit for the flight path change. In addition, it is important to consider other

factors such as the length of exposure time and the sensitivity of individuals exposed to particles.

In Figure 9, a red line is added to the drone's flight path, which is determined and indicates the change in flight path when the dust concentration exceeds 50 μg/m$^3$. The red line represents the drone's new path to avoid high dust concentration. The longitude and latitude are also updated in real time as the drone follows the new path. With GP2Y10, the results of creating a new route when the threshold is exceeded are obtained and elucidated. However, a process regarding the possibility of changing the route as a result of the measurement in a certain land and the specific measurements obtained in connection with the fulfillment of the task in the scanning area defined in the first section is defined for the UAV. From this point of view, firstly the search area and flight path are defined. Here, the scanning area is defined as a 10m x 10m rectangle divided into 25 sub-squares of 2m x 2m dimensions. The flight path is determined as a zigzag pattern that will cover the entire scanning area. After the area is determined, the GP2Y10 sensor is initialized. The GP2Y10 library in Python is used to interact with the sensor. Dust level is measured at every point of the flight path using the GP2Y10 sensor. The UAV is moved to the center of each subframe, measuring for a few seconds and moving to the next subframe. After collecting the data, the flight path and dust levels are plotted. The matplotlib library is used to plot the flight path and measured dust levels. The flight path becomes a zigzag pattern connecting the centers of the subframes. Dust levels are represented by colors in the chart.

**Figure 9**
**Planning the flight path in case the dust level rises above threshold**

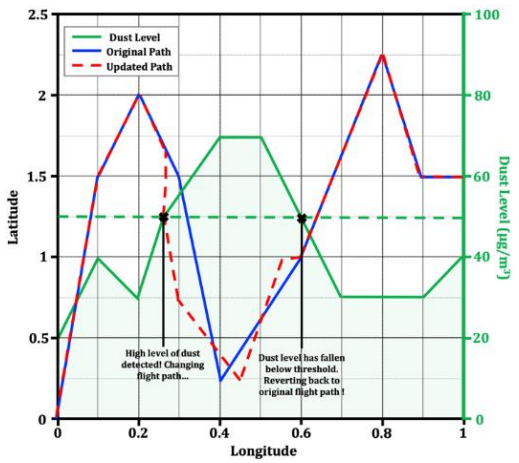


First, the flight path is defined as a list of x, and y coordinates. Next, *get_dust_level()* function is defined to obtain the dust level at the current location of the drone using the GP2Y10 sensor. The *move_to_next_position(x, y)* function is also defined to move the drone to the next position in the flight path. The main function *scan_area()* scans the entire area by moving the drone to each location on the flight path and storing the dust level at that location in a list called *dust_levels*. After scanning the area, a mesh grid is created for plotting and transforming the *dust_levels* list into a 2-dimensional array called *dust_levels_arr* which can be plotted as a heatmap. Finally, using *plt.pcolormesh()* plots the flight path as blue dots and dust levels as a heat map. The resulting plot shows the dust levels at each location in the flight path.

A hexacopter's trajectory is controlled by the GP2Y10 dust sensor and the Ublox M8N GPS module. The program scans a 10m x 10m square area using a zigzag pattern. The zone is divided into 25 sub-squares, each measuring 2m x 2m. The sensor measures the dust level in the center of each subframe. When the dust level is above 50 μg/m$^3$, the UAV maneuvers right or left or up to get out of the square, and when it reaches the other small square, it re-centers itself in the small square and scans it in a zigzag pattern. When the dust level is below 50 μg/m$^3$, the UAV continues to scan the area using the normal zigzag pattern. However, after the first scan is completed, the UAV returns to the starting point and increases the height by 50 meters and increases the height up to 200 meters by measuring 4 times at 50-meter intervals. This task code can be run through Mission Planner software using Python language. The UAV uses ArduPilot flight computer and Holybro Telemetry set. In addition, the program communicates with the UAV using the Mavlink protocol. To continue with the code, it is necessary to connect to the main control program of the UAV and configure all the sensors. Then, the UAV will scan the area with a zigzag pattern and when the dust level is above 50 μg/m$^3$ it will maneuver right or left or up out of the square. On the other hand, using some libraries that have been used in similar projects, the code can be written more quickly. For example, with a console application called MAVProxy by ArduPilot, it is integrated with pymavlink, a Python library used to communicate with ArduPilot. Using this library, it allows to create and send the necessary messages to control the UAV. Also, a library called OpenCV can help detecting the area and move in a zigzag pattern.

As shown in Figure 10a and 10b, the UAV has basically two different missions. First, it is necessary to follow a precise route with the GP2Y10 dust sensor, and monitor the dust level in the measuring area. Second, it is necessary to scan in a certain pattern. As a first step, the dust level is read from the GP2Y10 dust sensor and it is checked whether the measurement is higher than 50 μg/m$^3$. If the measurement is higher than 50 μg/m$^3$, the UAV needs to change course and move to the edge of the high dust level square, then move to the next frame to exit that square. If the measurement is less than 50 μg/m$^3$, the UAV scans the area and changes the flight path using the normal zigzag pattern as shown in Figure 10a. As a second step, the UAV needs to move up from the bottom left while scanning the measurement area, then apply the downward zigzag pattern on the right and top right corners. While scanning a square, the UAV is measuring the dust level and if it is higher than 50 μg/m$^3$ as shown in Figure 10b, it must change its course and move towards the edge of the square with high dust level, then move towards the next square to exit that square. Where the measurement is less than 50 μg/m$^3$, the UAV uses the normal zigzag pattern to scan the area and change the flight path.

## 4. Conclusion

In this study, an approach is developed to improve precise and intuitive solutions in an unmanned aerial vehicle (UAV) as a new use case for atmospheric dust sensors. Different missions have been generated and tested for the precise route through dust sensor measurements. To avoid areas with high dust levels that could pose a risk to humans, the autopilot detects particulate matter concentration and can direct it to fly to different locations with lower dust levels. During this process, flight speed, altitude, and sensitivity of the aerial vehicle to wind conditions are taken into account, and it is scanned according to the assigned mission area and initial position. As a result, the use of a UAV that performs measurements using an atmospheric dust sensor in precise route application provides benefits in many areas such as air quality measurement, forest fire monitoring, agricultural field survey, surveillance and rescue operations, and route planning. Thanks to this technology, it becomes possible for aerial vehicles to fly more accurately and to measure air pollution more accurately. In addition, the system used is especially important because it has a low budget and simple hardware structure, which makes it more accessible and useful. The developed approach not only enhances the efficiency of UAV operations in environmental sensing but also contributes to cost-effectiveness, enabling broader adoption and application of this technology in diverse settings.

**Figure 10**
**(a)Paths to be followed for measurements below threshold**

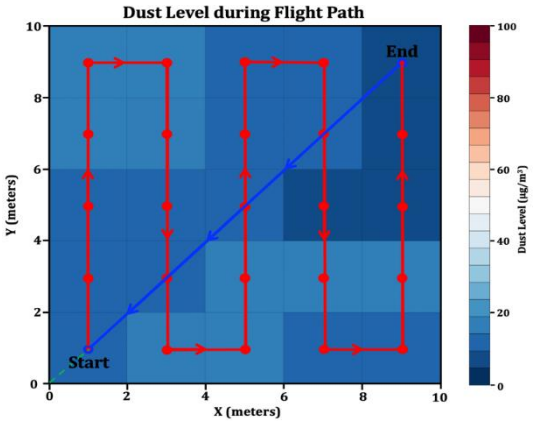


**(b)Paths to be followed for measurements above threshold**

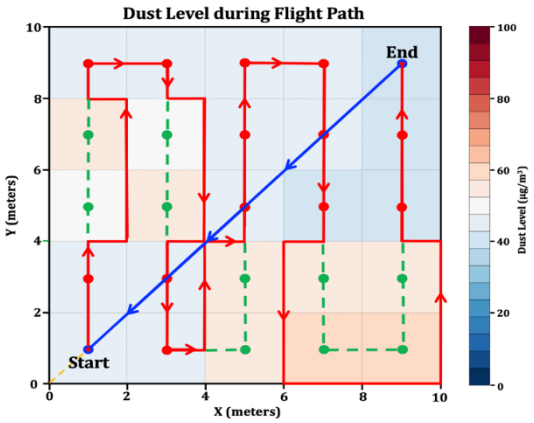


## Ethical Statement

This study does not contain any studies with human or animal subjects performed by any of the authors.

## Conflicts of Interest

The authors declare that they have no conflicts of interest to this work.

## Data Availability Statement

Data sharing is not applicable to this article as no new data were created or analyzed in this study.

## References

Aissaoui, R., Deneuville, J. C., Guerber, C., & Pirovano, A. (2023). A survey on cryptographic methods to secure communications for UAV traffic management. *Vehicular Communications, 44*, 100661. https://doi.org/10.1016/j.vehcom.2023.100661

Bakirci, M., & Ozer, M. M. (2023a). A low-cost UAV design for surveillance purposes in swarm systems. In *11th International Symposium on Digital Forensics and Security*, 1-6. https://doi.org/10.1109/ISDFS58141.2023.10131774

Bakirci, M., & Ozer, M. M. (2023b). Post-disaster area monitoring with swarm UAV systems for effective search and rescue. In *10th International Conference on Recent Advances in Air and Space Technologies*, 1-6. https://doi.org/10.1109/RAST57548.2023.10198022

Cui, Z., & Wang, Y. (2021). UAV path planning based on multi-layer reinforcement learning technique. *IEEE Access, 9*, 59486-59497. https://doi.org/10.1109/ACCESS.2021.3073704

Hossain, N.U.I., Sakib, N., Govindan, K. (2022). Assessing the performance of unmanned aerial vehicle for logistics and transportation leveraging the Bayesian network approach. *Expert Systems with Applications*, 209, 118301. https://doi.org/10.1016/j.eswa.2022.118301

Jońca, J., Pawnuk, M., Bezyk, Y., Arsen, A., & Sówka, I. (2022). Drone-assisted monitoring of atmospheric pollution - A comprehensive review. *Sustainability*, *14*(18), 11516. https://doi.org/10.3390/su141811516

Lambey, V., & Prasad, A. D. (2021). A review on air quality measurement using an unmanned aerial vehicle. *Water, Air, & Soil Pollution*, *232*(3), 109. https://doi.org/10.1007/s11270-020-04973-5

Li, B., Yang, Z., Chen, D., Liang, S., & Ma, H. (2021). Maneuvering target tracking of UAV based on MN-DDPG and transfer learning. *Defence Technology*, *17*(2), 457-466. https://doi.org/10.1016/j.dt.2020.11.014

Li, Y., Liu, M., & Jiang, D. (2022). Application of unmanned aerial vehicles in logistics: A literature review. *Sustainability*, *14*(21), 14473. https://doi.org/10.3390/su142114473

Loli, M., Mitoulis, S.A., Tsatsis, A., Manousakis, J., Kourkoulis, R., Zekkos, D. (2022). Flood characterization based on forensic analysis of bridge collapse using UAV reconnaissance and CFD simulations. *Science of The Total Environment*, 822, 153661. https://doi.org/10.1016/j.scitotenv.2022.153661

Malamiri, H.R.G., Aliabad, F.A., Shojaei, S., Morad, M., Band, S.S. (2021). A study on the use of UAV images to improve the separation accuracy of agricultural land areas. *Computers and Electronics in Agriculture*, 184, 106079. https://doi.org/10.1016/j.compag.2021.106079

Masuduzzaman, M., Islam, A., Sadia, K., Shin, S.Y. (2022). UAV-based MEC-assisted automated traffic management scheme using blockchain. *Future Generation Computer Systems*, 134, 256-270. https://doi.org/10.1016/j.future.2022.04.018

Puente-Castro, A., Rivero, D., Pazos, A., & Fernandez-Blanco, E. (2022). A review of artificial intelligence applied to path planning in UAV swarms. *Neural Computing and Applications*, *34*(1), 153-170. https://doi.org/10.1007/s00521-021-06569-4

Ramachandran, A., & Sangaiah, A. K. (2021). A review on object detection in unmanned aerial vehicle surveillance. *International Journal of Cognitive Computing in Engineering*, *2*, 215-228. https://doi.org/10.1016/j.ijcce.2021.11.005

Song, B. D., Park, K., & Kim, J. (2018). Persistent UAV delivery logistics: MILP formulation and efficient heuristic. *Computers & Industrial Engineering*, *120*, 418-428. https://doi.org/10.1016/j.cie.2018.05.013

Sziroczak, D., Rohacs, D., & Rohacs, J. (2022). Review of using small UAV based meteorological measurements for road weather management. *Progress in Aerospace Sciences*, *134*, 100859. https://doi.org/10.1016/j.paerosci.2022.100859

Villa, T. F., Gonzalez, F., Miljievic, B., Ristovski, Z. D., & Morawska, L. (2016). An overview of small unmanned aerial vehicles for air quality measurements: Present applications and future prospectives. *Sensors*, *16*(7), 1072. https://doi.org/10.3390/s16071072

Wang, Y., Li, K., Han, Y., & Yan, X. (2022). Distributed multi-UAV cooperation for dynamic target tracking optimized by an SAQPSO algorithm. *ISA Transactions*, *129*, 230-242. https://doi.org/10.1016/j.isatra.2021.12.014

Xin, L., Tang, Z., Gai, W., & Liu, H. (2022). Vision-based autonomous landing for the UAV: A review. *Aerospace*, *9*(11), 634. https://doi.org/10.3390/aerospace9110634

Yu, Q., & Xing, G. (2021). Application and development of UAV in emergency rescue in our country. *Occupational Health and Emergency Rescue*, *39*(3), 350-355. https://doi.org/10.16369/j.oher.issn.1007-1326.2021.03.024

How to Cite: Martinez, R., & Morales, A. (2024). Real Time Route Adjustment of a UAV Based on Dust Measurement with an Onboard Sensor. Archives of Advanced Engineering Science. https://doi.org/10.47852/bonviewAAES42021702